Available online at www.eccomasproceedia.org
Eccomas Proceedia COMPDYN (2017) 4393-4407

ECCOMAS
Proceedia

COMPDYN 2017
6th ECCOMAS Thematic Conference on
Computational Methods in Structural Dynamics and Earthquake Engineering
M. Papadrakakis, M. Fragiadakis (eds.)
Rhodes Island, Greece, 15–17 June 2017

INNOVATIVE DEVICES FOR THE BASE ISOLATION OF EXISTING BUILDINGS

F. Fabbrocino[1], M. Titirla[2], A. Amendola[2], G.Benzoni[3], F. Fraternali[2]

[1]Pegaso University, Department of Engineering, 80132 Naples, Italy
francesco.fabbrocino@unipegaso.it (F. Fabbrocino)

[2] Department of Civil Engineering, University of Salerno, 84084 Fisciano (SA), Italy
titirlamagdalini@gmail.com (M. Titirla), adaamendola1@unisa.it (A. Amendola),
f.fraternali@unisa.it (F. Fraternali),

[3]Department of Structural Engineering, University of California San Diego, San Diego, CA 92161, USA. gbenzoni@ucsd.edu (G. Benzoni)

Keywords: Seismic Isolation; Historical buildings; Pentamode Lattices

Abstract

It is well known that pre-existing buildings are often inadequate to resist strong ground motions, and that their seismic rehabilitation is not an easy task. Several studies available in the to-date literature have shown that seismic isolation is a cost-effective and efficient method that can be employed to protect existing structures from earthquakes. A new class of performance-based seismic isolators has been proposed in recent studies, making use of pentamode lattices confined between stiffening plates. The present work illustrates experimental results concerned with shear and compression tests on physical (reduced-scale) models of pentamode bearings, and discusses the use of such systems for the base isolation of existing buildings. Given results highlight the special ability of such systems to behave as tension-capable and performance-based systems, whose mechanical properties are driven largely by the geometry of the lattice microstructure (i.e, such systems behave as mechanical metamaterials), and can be finely adjusted to the properties of the structure to be protected.

Peer-review under responsibility of the organizing committee of COMPDYN 2017.
doi: 10.7712/120117.5732.17771

1. INTRODUCTION

Extremal materials that are receiving increasing interest are the so-called pentamode lattices, which consist of diamond-like lattices featuring five soft modes of deformation (unit cell with four rods meeting at a point) [1]. Such lattices exhibit very low shear moduli (theoretically equal to zero) [1], and may be able to stop or dramatically attenuate shear waves [2]. Physical models of pentamode materials have been fabricated through additive manufacturing (AM) techniques over the last few years, both at the macro- [3] and at the micro-scale [3]. Schittny et al. [3] have studied the experimental behavior of macroscopic, polymeric samples of pentamode lattices in the elastic regime: the results obtained by such authors prove that the elastic moduli of pentamode materials are strongly related to the geometry of the lattice micro-structure, being markedly affected by the dimensions of the rods forming the lattice, and particularly sensitive to the ratio between the diameter d of the connections between the rods and the lattice constant a. The experimental Young's modulus E of the lattice has been found approximately three times stiffer than the experimental shear modulus G. The results presented in [3] also show that the ratio between the bulk modulus B and the shear modulus G strongly increases by reducing the contact area between the rods. Similar results have been found at the microscale by Kadic et al. [3]. Polymeric samples of pentamode lattices have been fabricated by such authors using dip-in direct-laser-writing (DLW) optical lithography, a technique well suited to build three-dimensional structures across a range of scales from micro to small [5]. Experimental and numerical results given in [3] and [3] demonstrate that the mechanical behavior of pentamode lattices replicates that of fluids in the limit of $d \to 0$, when the shear modulus G tends to zero. For finite, nonzero values of d, it has been found that the B/G ratio is extremely high, even if G is positive and nonzero [3][3]. Because of their unusual mechanical features, pentamode materials have been proposed for transformation acoustics and elasto-mechanical cloak (refer, e.g., to the recent paper [6] and the references therein), but their potential in different engineering fields is still only partially explored.

The present study investigates the elastic and post-elastic responses of additively manufactured pentamode lattices confined between stiffening plates. We analyze metallic samples obtained through additive manufacturing by Electron Beam Melting (EBM) of a powder of the titanium alloy Ti-6Al-4V [7][8][9], for different aspect ratios of the unit-cell, and two macroscale aspect ratios (slender and thick samples). We find that the confinement of pentamode lattices between stiffening plates greatly affects the elastic response of the overall structure, compared with the case of unconfined, infinite pentamode lattices [10]. The obtained results highlight several similarities between the elastic response of confined pentamode materials and the analogous response of elastomeric bearings composed of rigid steel or fiber-reinforced composite layers and soft layers of natural or synthetic rubber [11]-[17]. Concerning the post-elastic response, we observe that the examined pentamode materials feature acceptable energy dissipation capacity, and ranges of supplemental damping in line with values of common isolation devices. Their use for the base isolation of existing buildings is discussed.

2. MATERIALS AND METHODS

2.1 Physical models of confined pentamode materials

We manufactured pentamode lattices confined by stiffening plates and made by the titanium alloy Ti-6Al-4V (hereafter simply denoted by Ti6Al4V) through the Arcam S12 EBM facility at the Department of Materials Science and Engineering, University of Sheffield. Such an additive manufacturing (AM) technology allows the manufacture of features with size down to 0.4 mm by progressively depositing, heating and melting layers of Ti6Al4V powder, with the

melted regions in each layer defined according to a CAD model of the specimen to be manufactured [7][8]. It is worth noting that the size of the specimen designed by CAD does not correspond perfectly to the built object. The beam scan strategies and the surface roughness will result in larger (in diameter) printed members [9]. The main properties of the employed titanium alloy, when in the fully dense state, are given in Table 1 [18].

mass density [g/cm^3]	4.42
yield strength [MPa]	910.00
Young's modulus [GPa]	120.00
Poisson's ratio	0.342

Table 1. Main physical and mechanical properties of the fully dense isotropic polycrystalline Ti6Al4V titanium alloy [18].

Figure 1 shows the extended face-centered-cubic (fcc) unit cell of a pentamode lattice formed by sixteen rods that are composed of two truncated bi-cones featuring large diameter D at the mid-span and small diameter d at the extremities [2][3][3][5][6]. Upon selecting the lattice constant $a = 30$ mm and $D = 2.72$ mm ($D/a \approx 9\%$), we manufactured pentamode specimens with the unit cell shown in Figure 1, using three different values of d: $d_1 = 0.49$ mm ($d_1/a = 1.6\%$); $d_2 = 1.04$ mm ($d_2/a = 3.5\%$); and $d_3 = 1.43$ mm ($d_3/a = 4.8\%$, cf. Table 2). It is worth remarking that the limit $d/a \to 0$ corresponds to a perfectly pin-jointed lattice (stretching-dominated response), while the case with $d/a > 0$ corresponds to a lattice featuring nonzero bending rigidities of nodal junctions and rods, which deforms through both stretching of rods and bending of rods and nodes [10].

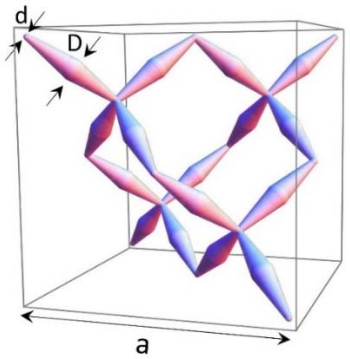

Figure 1. Extended fcc unit cell of the pentamode lattices analyzed in the present study.

	a [mm]	D [mm]	d_1 [mm]	d_2 [mm]	d_3 [mm]
Built size	30	2.72	0.49	1.04	1.43
(CAD size)	(30)	(2.71)	(0.45)	(0.90)	(1.35)

Table 2. Geometrical parameters of the EBM built pentamode materials (CAD sizes in brackets).

We additively manufactured two different sets of pentamode specimens:

(a) *"Slender Pentamode Materials"* (SPM): obtained by replicating the extended fcc unit cell of Figure 1 $2x2$ times in the horizontal plane, 4 times along the vertical axis, and confining the $2x2x4$ lattice between Ti6Al4V plates with 80 mm edge and $t_p = 1$ mm thickness (see Figure 2);

(b) *"Thick Pentamode Materials"* (TPM): obtained by replicating the extended fcc unit cell of Figure 1 $2x2$ times in the horizontal plane, 2 times along the vertical axis, and confining the $2x2x2$ lattice between the above mentioned plates (see Figure 3).

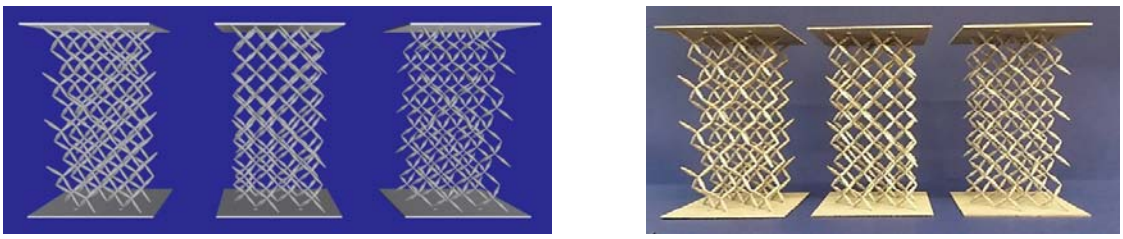

(a) (b)

Figure 2. CAD (a) and EBM (b) models of slender (SPM) specimens ($2x2x4$ extended unit cells).

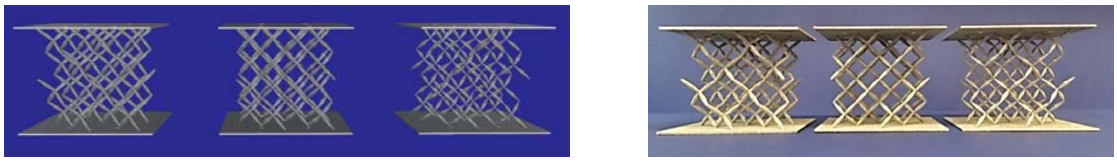

(a) (b)

Figure 3. CAD (a) and EBM (b) models of thick (TPM) specimens ($2x2x2$ extended unit cells).

Hereafter, we name SPM1, SPM2 and SPM3 the SPM-specimens with $d = d_1$, $d = d_2$, and $d = d_3$, respectively. Similarly, TPM1, TPM2 and TPM3 $d = d_1$, $d = d_2$, and $d = d_3$, respectively. We built three different SPM specimens and one TPM specimen for each analyzed d/a ratio. It is well known that the EBM manufacturing process creates solid material with some level of porosity (typically below 0.2% if suitable parameters for the alloy are used in the machine) instead of fully dense materials for both solid structures [9] and those intended to contain free space [8]. Based on a recent, detailed study of porosity in EBM titanium made with the same conditions used for the current material [9], we hereafter assume the internal porosity of such a material is of the order of 0.2%, and its Young modulus E_m is therefore approximately equal to that of the fully dense Ti6Al4V alloy (Table 1).

2.2 Experimental setup

An in-house experimental setup was assembled to apply lateral force-displacement histories under constant vertical load on the pentamode specimens described in the previous section (Figure 4).

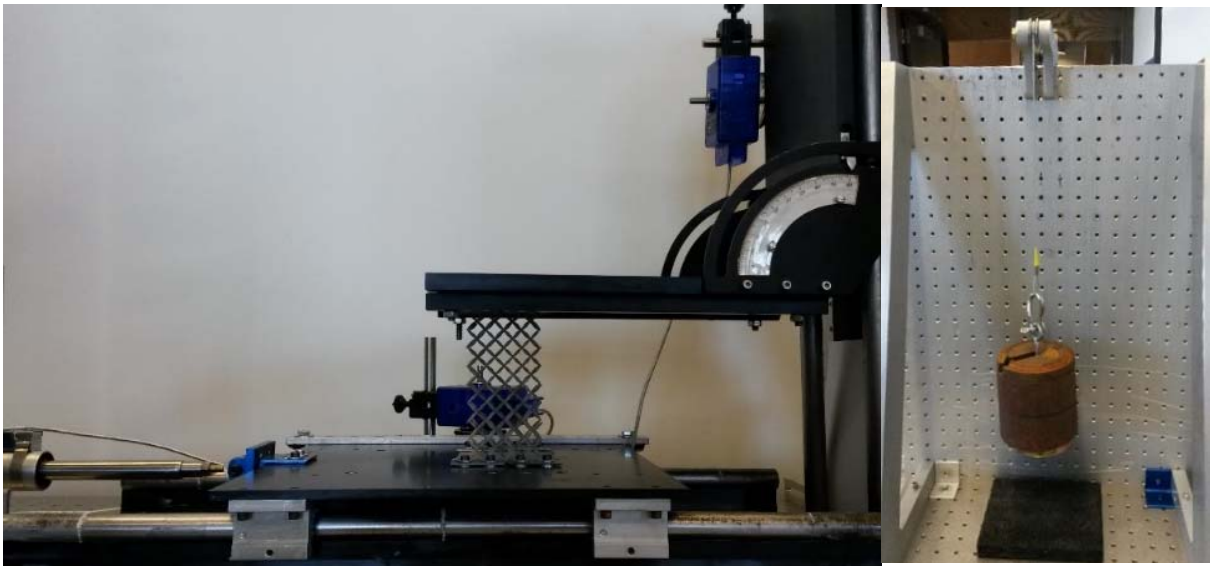

Figure 4. Left: overall view of the experimental setup. Right: counter balancing system introduced to remove platen self-weight.

An L-shaped plate, sliding vertically over linear bearings, allows the application of the vertical load through calibrated weights. The selfweight of the plate is removed with a counter balancing system of pulley and weights (Figure 4). The top base of the specimen is firmly connected to the plate by clamping strips located all around the base edges. The same clamping mechanism is applied to the bottom base of the specimen that is connected to the horizontally sliding table (Figure 5). Horizontal displacements are applied through an actuator connected to the sliding table and reacting against a solid metal block. The force rating of the actuator is 300 lb (1.3 kN), with a displacement range of +/-100 mm. Forces are acquired by a load cell installed between the back of the actuator and the reaction block. Vertical and lateral displacements are measured with rotary motion sensors.

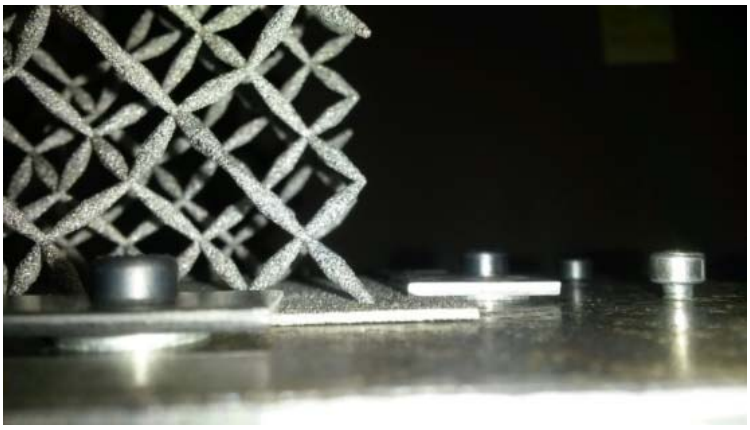

Figure 5. Connection of the specimen to the sliding table.

The same setup allows the application of the vertical load through calibrated weights while no horizontal motion is applied. With this procedure compression tests were completed by manual application of weights and automatic recording of vertical displacements of the plate. Preliminary to any actual test, the setup was subjected to a shakedown phase to assess the frictional force components and to verify alignments and parallelisms. The test data were consistently processed with the removal of friction from the testing equipment.

3. EXPERIMENTAL RESULTS

The present section illustrates the results of the laboratory tests that we conducted to characterize the mechanical response of the pentamode materials illustrated in Sect. 2.1. We begin by estimating the elastic moduli of slender and thick pentamode materials through cyclic lateral force-displacement tests at constant vertical loading, and monotonic vertical force-displacement tests under zero horizontal force. Next, we investigate the inelastic response of the analyzed materials via (cyclic and monotonic) lateral force-displacement tests conducted up to specimen's failure. Figure 6 illustrates pictures of selected slender and thick specimens extracted from in-situ videos of lateral force-displacement tests.

We investigated the post-elastic response of SPM and TPM specimens by conducting cyclic lateral force - displacement tests in displacement control up to specimen's failure (under the vertical load $F_v = 44.45$N, and the strain rate $\dot{\delta}_h = 0.8$ mm/sec, cf. Figure 7-Figure 8). In the case of SPM specimens, we also performed monotonic lateral force-displacement tests up to specimen's failure (Figure 7). All such tests were carried out starting from the virgin state, for a single specimen of each microstructure aspect ratio d/a (cf. Sect. 2.1). Figure 7 shows the measured envelope force– displacement F_h-δ_h curves, where the labels a,b and c indicate the final point of the initial linear branch, the peak of horizontal force and the failure point, respectively. For these specimens, point c corresponds to the ultimate vertical bearing capacity. The actual F_h-δ_h curves of the monotonic tests on SPM specimens showed marked oscillations in the unstable phase characterized by a decrease of F_h for increasing values of δ_h, due to progressive joint failure. The final collapse of the specimen occurred due to the rupture of several terminal nodes placed along the stretched diagonals (Figure 9).

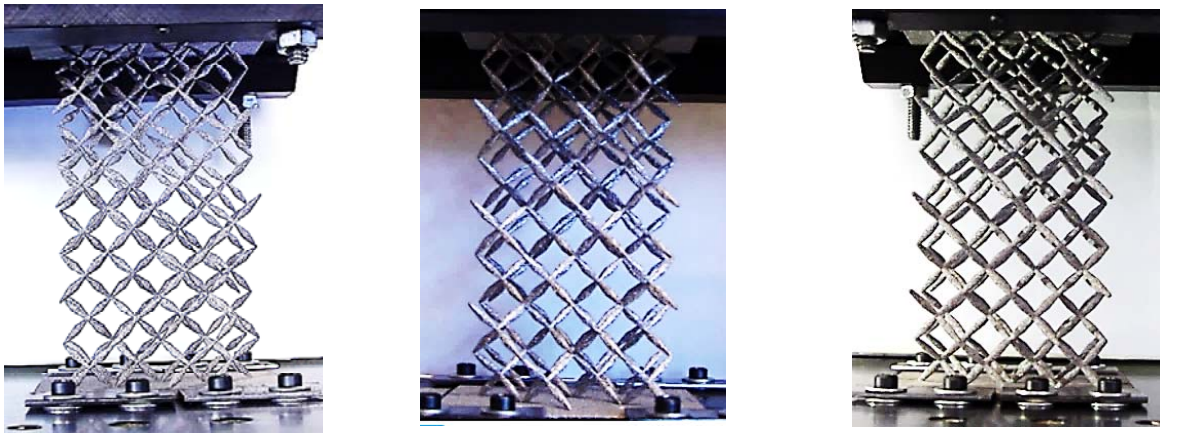

(a): SPM1 (b): SPM2 (c): SPM3

(d): TPM1 (e): TPM2 (f): TPM3

Figure 6. Frames from in-situ videos of lateral displacement tests on SPM and TPM specimens.

The results in Figure 7 highlight an initial hardening branch of the post-elastic response of each examined specimen. Such a branch is followed by a second post-elastic branch with negative tangent stiffness, which progressively leads the specimen to collapse. The coordinates of the above *a-b-c* points are provided in Table 3, together with the ductility values computed as follows

$$\mu = \frac{\delta_h - \delta_{h,el}}{\delta_{h,el}} \tag{6}$$

where δ_h is the current value of the lateral displacement, and $\delta_{h,el}$ is the lateral displacement in correspondence to point a.

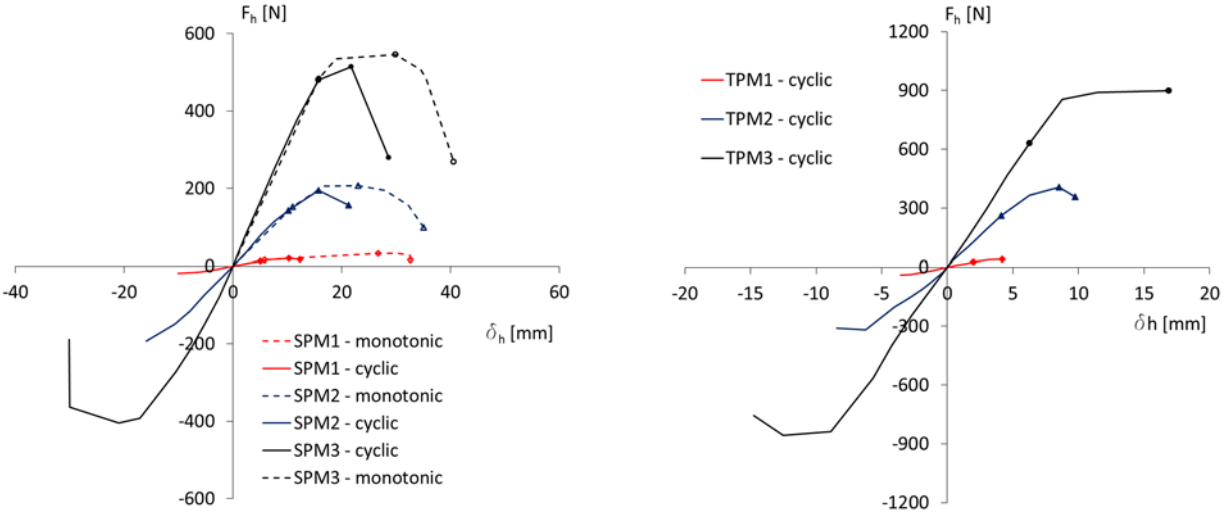

Figure 7. Measured envelops of cyclic (solid lines) and monotonic (dashed lines) lateral force-displacement tests.

		F_a	δ_a	μ_a	F_b	δ_b	μ_b	F_c	δ_c	μ_c
		[N]	[mm]		[N]	[mm]		[N]	[mm]	
SPM1	monotonic	15.92	5.85	1.00	32.93	26.74	4.57	16.20	32.67	5.58
	cyclic	12.70	5.02	1.00	20.19	10.29	2.06	17.67	12.35	2.47
SPM2	monotonic	152.38	10.98	1.00	206.83	22.97	2.09	100.01	35.03	3.19
	cyclic	143.10	10.23	1.00	195.12	15.75	1.54	157.03	21.26	2.07
SPM3	monotonic	485.01	15.79	1.00	545.56	29.92	1.89	268.5	40.64	2.57
	cyclic	480.12	15.70	1.00	514.00	21.70	1.38	280.00	28.65	1.82
TPM1	cyclic	25.22	2.00	1.00	40.20	4.17	2.08	40.20	4.17	2.08
TPM2	cyclic	262.18	4.11	1.00	407.34	8.53	2.07	357.45	9.76	2.37
TPM3	cyclic	467.93	4.55	1.00	899.02	16.88	2.70	899.02	16.88	2.70

Table 3. Coordinates and ductility values of noticeable points of the curves in Figure 7.

The cyclic tests in Figure 8 where performed at controlled ductility on a SPM1 and a TPM3 specimen, by letting the maximum lateral displacement to grow progressively in such a way that it results $\mu = 0.25$ in the first cycle; μ grows with step 0.25 in the next cycles up to $\mu = 1.00$; and, finally, μ grows with step 0.50 in the post-elastic cycles up to specimen's failure. Figure 7-left shows a comparison between the measured envelopes of cyclic tests and monotonic tests on SPM specimens, which highlights the fact that the envelopes of the monotonic tests always lie above those of the cyclic tests in the post-elastic range, due to (low-cycle) fatigue-damage [13].

Post-yield stiffness degradation is a common observation in a range of different tests and lattice designs of EBM manufactured Ti6Al4V porous structures (e.g [8][9]), due to progressive brittle fracture of individual struts of the lattice from the point of first macroscopic yield [7].

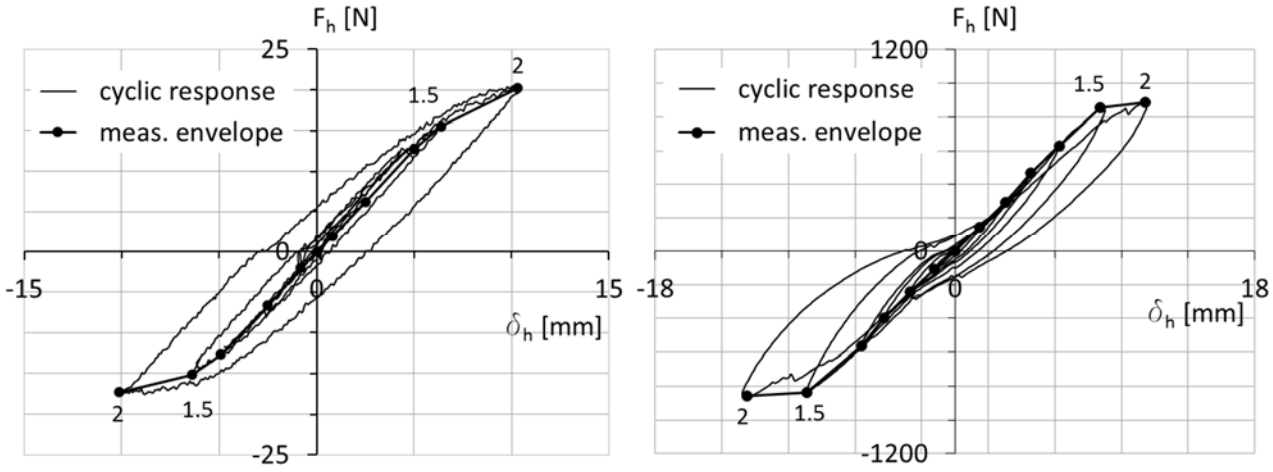

(a) (b)

Figure 8. Lateral force - displacement responses of a SPM1 (a) and a TPM3 (b) specimen under cyclic tests at constant vertical load $F_v = 45.34$ N (solid curves: measured envelope curves; numbers indicate ductility).

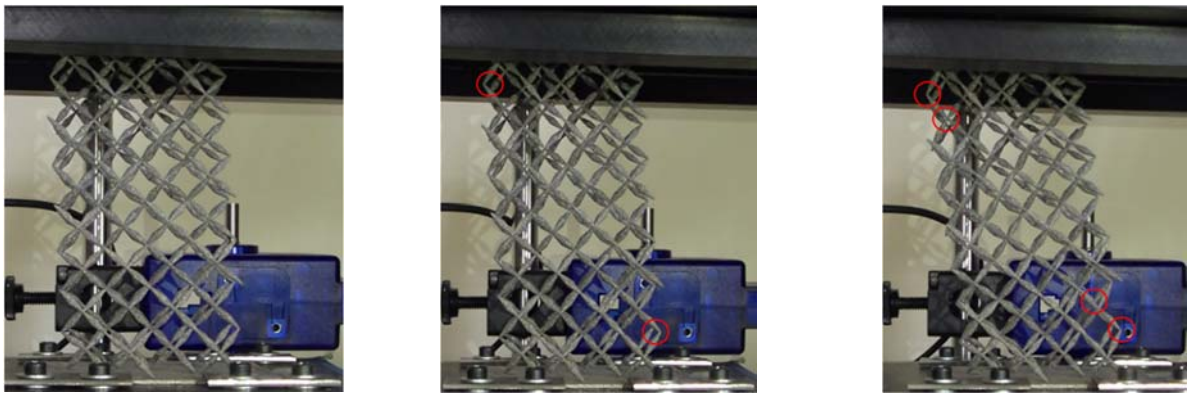

(a) SPM1 – *3rd elastic cycle* $\delta_h = 5.12$ mm, $\mu = 1.0$

(b) SPM1 - *1st inelastic cycle* $\delta_h = 6.40$ mm, $\mu = 1.5$

(c) SPM1 - *2nd inelastic cycle* $\delta_h = 10.29$, $\mu = 2.0$

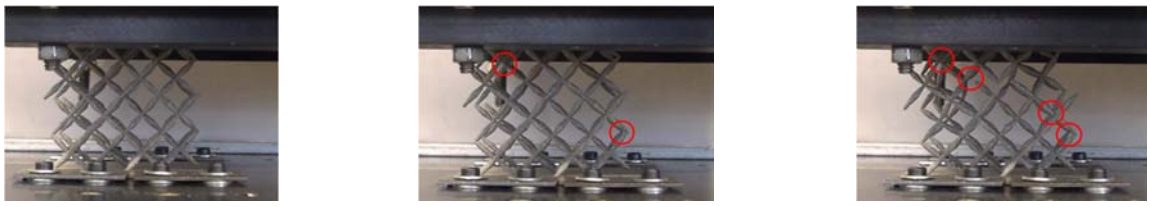

(d) TPM3 - *4th elastic cycle* $\delta_h = 6.25$ mm, $\mu = 1.0$

(e) TPM3 - *1st inelastic cycle* $\delta_h = 8.74$ mm, $\mu = 1.5$

(f) TPM3 - *2nd inelastic cycle* $\delta_h = 11.45$ mm, $\mu = 2.0$

Figure 9. Frames from in-situ videos of lateral displacement tests on a SPM1 (a-b-c) and a TPM3 (d-e-f) specimen. The circled struts are affected by fracture damage.

Table 7 shows the Energy Dissipated per Cycle EDC the effective viscous damping ξ_{eff}; the post-yield (K_d) vs. elastic (K_e) stiffness ratio $|K_d - K_e|/K_e$; and characteristic strength Q_d defined as force at zero horizontal displacement (cf. point 8.2.1.2.2 of [24]).

		EDC ($10^3\,kN\cdot mm$)	ξ_{eff} (%)	$\lvert K_d - K_e\rvert / K_e$ (%)	Q_d (N)
SPM1	$\mu_{\max}=1.5$	191.44	25.11	25.73	1.52
	$\mu_{\max}=2.0$	406.27	31.12	57.44	5.27
TPM3	$\mu_{\max}=1.5$	$12.97\cdot 10^3$	28.02	10.07	93.12
	$\mu_{\max}=2.0$	$18.86\cdot 10^3$	30.12	88.73	95.01

Table 4. Energy dissipation per cycle (E_{diss}); effective viscous damping (ξ_{eff}); post-yield vs. elastic stiffness ratio ($\lvert K_d - K_e\rvert / K_e$); and characteristic strength (Q_d) at different post-elastic cycles of lateral force – displacement test on SPM1 and TPM3 specimens.

The effective damping in Table 7 is defined in line with the European standard on anti-seismic devices EN 15129:2009 [24], and corresponds to the energy dissipated E_{diss} through the following formula

$$\xi_{eff} = \frac{E_{diss}}{2\pi K_{h,eff}\,\delta_{h,\max}^2} \tag{5}$$

where $K_{h,eff}$ is the effective secant stiffness, and $\delta_{h,\max}$ is the maximum lateral displacement of the current cycle (see point 3.1.10 of [24]). The results in Table 7 highlight progressive increases of ξ_{eff}, $\lvert K_d - K_e\rvert / K_e$, and Q_d with the amplitude of the maximum lateral displacement (i.e., with $\mu_{\max}$), due to progressive fracture of lattice struts [8] (cf. Figure 9). The results in terms of energy dissipated per cycle (and effective damping) while indicating a progressive increase with displacement show also values of supplemental damping (25% to 30%) that are suitable for seismic isolation applications. The failure mechanisms in Figure 9 indicate a quite symmetric pattern of broken elements between top and bottom of the specimen. It was also observed that during the tests the failure of struts happened in a rather smooth progression and in expected locations. This performance new configurations that can significantly increase the required structural ductility to be forseen.

3 CONCLUDING REMARKS

We have experimentally investigated the response of EBM printed Ti6Al4V specimens of pentamode materials confined between stiffening plates, under lateral and vertical force-displacement tests. The examined tests were aimed at researching the effective shear and compression properties of such systems, and their inelastic response under cyclic and monotonic loading histories. We have examined a collection of specimens that differ in microstructural and macrostructural aspect ratios, which are related to the size of the nodal junctions (microstructure aspect ratio) and the ratio between the number of unit cells placed in the vertical and horizontal directions (macrostructure aspect ratio).

Several results of the present study highlight analogies between the mechanical response of the analyzed systems and that of elastomeric bearings consisting of alternating layers of synthetic or natural rubber and stiffening layers made of steel plates or fiber-reinforced composites, which are commonly used as bridge support devices or seismic or vibration isolators for buildings [11]-[17]. We have observed that the ratio between the effective compression

modulus E_{eff} and the effective shear modulus G_{eff} of the analyzed pentamode materials is markedly affected by the presence of the stiffening plates, as compared to available theoretical predictions of the E/G ratio of unconfined pentamode lattices [10] ($E/G \approx 1.0$). Such a stiffening effect is larger in the case of slender specimens and large-size nodal junctions, since the E_{eff}/G_{eff} ratio varies between 7.93, in case of the SPM3 specimen, and 2.96, in case of the TPM1 specimen. It replicates the stiffening role played by steel layers in elastomeric bearings. It is worth noting, however, that the absolute vertical and lateral stiffness coefficients of the examined pentamode materials increase when passing from slender to thick specimens.

Despite the very preliminary nature of this study on feasibility for base isolation applications, some observations support the potential of pentamode structures for use in anti-seismic system development and/or as shear-wave band gap systems [2], with special attention to the isolation of existing buildings. The strict dependency of the response by the geometry of the lattice allows the design of structures of controlled performance. The ranges of supplemental damping observed for the specimens are well in line with values of common isolation devices. The levels of energy dissipated is acceptable and could be significantly improved by reducing material porosity, using different construction techniques, materials, and/or through the insertion of dissipative lead-cores within the pentamode isolator [11][14]. Additional horizontal ductility and vertical stiffness is expected to be developed also using different configurations that will provide more confinement to the single layers of the pentamode structure.

We address the design and modeling of highly dissipative pentamode bearings and impact mitigation devices to future work, on employing either manual assembling procedures [26], layered structures showing different materials and/or lattice geometries in different layers, and additive manufacturing techniques in polymeric and metallic materials [3][3][7]. We also address researches on the use of pentamode lattices within a large variety of materials and structures to future studies [58]-[60].

REFERENCES

[1] G.W. Milton, A.V. Cherkaev, Which Elasticity Tensors are Realizable?, *Journal of Engineering Materials and Technology*, **117**(4), 483-493, 1995.

[2] Martin A., Kadic M., Schittny M., Bückmann T., Wegener M., Phonon band structures of three-dimensional pentamode metamaterials, *Physical Review B*, **86**, 155116, 2010.

[3] M. Schittny, T. Bückmann, M. Kadic, M. Wegener, Elastic measurements on macroscopic three-dimensional pentamode metamaterials. *Applied Physics Letters*, **103**, 231905, 2013.

[4] M. Kadic, T. Bückmann, N. Stenger, M. Thiel, M. Wegener, On the practicability of pentamode mechanical metamaterials, *Applied Physics Letters*, **100**:191901, 2012.

[5] T. Buckmann, N. Stenger, M. Kadic, J. Kaschke, A. Frölich, T. Kennerknecht, C. Eberl, M. Thiel, M. Wegener, Tailored 3D Mechanical Metamaterials Made by Dip-in Direct-Laser-Writing Optical Lithography. *Advanced Materials*, **24**(20):2710-4, 2012.

[6] T. Bückmann, M. Thiel, M. Kadic, R. Schittny, M. Wegener, An elastomechanical unfeelability cloak made of pentamode metamaterials. *Nature Communications*, **5**:4130, 2014.

[7] A. Amendola, E.H. Nava, R. Goodall, I. Todd, R.E. Skelton, F. Fraternali, On the additive manufacturing and testing of tensegrity structures. *Composite Structures*, **131**, 66-71, 2015.

[8] E. Hernandez-Nava, C.J. Smith, F. Derguti, S. Tammas-Williams, F. Leonard, P.J. Withers, I. Todd, R. Goodall, The effect of density and feature size on mechanical properties of isostructural metallic foams produced by additive manufacturing. Acta Materialia, **85**, 387-395, 2015.

[9] S. Tammas-Williams, H. Zhao, F. Léonard, F. Derguti, I. Todd, PB. Prangnell, XCT analysis of the influence of melt strategies on defect population in Ti–6Al–4V components manufactured by Selective Electron Beam Melting. Materials Characterization, **102**, 47-61, 2015.

[10] W. van Grunsven, E. Hernandez-Nava, G.C. Reilly, R. Goodall, Fabrication and mechanical characterisation of titanium lattices with graded porosity. Metals, **4**(3), 401-9, 2014.

[11] A.N. Norris, Mechanics of elastic networks. Proceedings of the Royal Society of London A, **470**(522):1-18, 2014.

[12] M.C. Constantinou, A.S. Whittaker, Y. Kalpakidis, D.M. Fenz, G.P. Warn, Performance of seismic isolation hardware under service and seismic loading, Technical Report MCEER-07-0012, 2007.

[13] R.I. Skinner, W.H. Robinson, G.H. McVerry, An introduction to seismic isolation. Wiley, 1993.

[14] J.M. Kelly, Earthquake-resistant design with rubber. London: Springer-Verlag, 1993.

[15] G. Benzoni, C. Casarotti, Effects of vertical load, strain rate and cycling on the response of lead-rubber seismic isolators. *Journal of Earthquake Engineering*, **13**(3), 293-312, 2009.

[16] H. Toopchi-Nezhad, M.J. Tait, R.G., Drysdale Bonded versus unbonded strip fiber reinforced elastomeric isolators: Finite element analysis. *Composite Structures*, **93**(2), 850-859, 2014.

[17] P.M. Osgooei, M.J. Tait, D. Konstantinidis, Three-dimensional finite element analysis of circular fiber- reinforced elastomeric bearings under compression. *Composite Structures* **108**(1), 191-204, 2014.

[18] P.M. Osgooei, M.J. Tait, D. Konstantinidis, Finite element analysis of unbonded square fiber-reinforced elastomeric isolators (FREIs) under lateral loading in different directions. *Composite Structures* **113**(1):164-173, 2014.

[19] Metals Handbook, (2) Properties and selection: nonferrous alloys and special-purpose materials. ASM International, Metals Park, OH, 1990.

[20] L.R. Meza, S. Das, J.R. Greer, Strong, light weight, and recoverable three-dimensional ceramic nanolattices. *Science* **6202**(345):1322-1326, 2014.

[21] VS Deshpande, NA Fleck, MF.Ashby, Effective properties of the octet-truss lattice material. *Journal of the Mechanics and Physics of Solids*, **22**, 409-428, 2001.

[22] T.A. Schaedler, A.J. Jacobsen, A. Torrents, A.E. Sorensen, J. Lian, J.R. Greer, L. Valdevit, W.B. Carter. Ultralight Metallic Microlattices. *Science* **6058**(334), 962-965, 2011.

[23] R.K. Steele, A.J. McEvily, The high-cycle fatigue behavior of Ti-6Al-4V alloy. *Engineering Fracture Mechanics,* **8**, 31-37, 1976.

[24] I. Szachogluchowicz, L. Sniezek, V. Hutsaylyuk, Low cycle fatigue properties laminate AA2519-TI6AL4V. *Procedia Engineering*, **114**, 26-33, 2015.

[25] European Committee for Standardization. Anti-seismic devices, EN 15129. Brussels, Belgium, 2009.

[26] Atlas of stress-strain curves, 2nd Edition, ASM International, Materials Park, OH, 2002.

[27] A. Amendola, G. Carpentieri, M. de Oliveira, R.E. Skelton, F. Fraternali, Experimental investigation of the softening stiffening response of tensegrity prisms under compressive loading. *Composite Structures*, **117,** 234-243, 2014.

[28] B. Schmidt, F. Fraternali, Universal formulae for the limiting elastic energy of membrane networks, *Journal of the Mechanics and Physics of Solids*, **60**, 172-180, 2012.

[29] L. Ascione, F. Fraternali, A penalty model for the analysis of composite curved beams, *Computers & Structures*, **45**, 985-999, 1992.

[30] F. Fraternali, J.N. Reddy, A penalty model for the analysis of laminated composite shells, *International Journal of Solids and Structures*, **30**, 3337-3355, 1993.

[31] F. Fraternali, Free Discontinuity Finite element models in two-dimensions for in-plane crack problems*, Theoretical and Applied Fracture Mechanics*, **47**, 274-282, 2007.

[32] F. Fraternali, C.D Lorenz, G. Marcelli, On the estimation of the curvatures and bending rigidity of membrane networks via a local maximum-entropy approach, *Journal of Computational Physics*, **231**, 528-540, 2012.

[33] F. Fraternali, G. Bilotti, Non-Linear Elastic Stress Analysis in Curved Composite Beams. *Computers & Structures*, **62**, 837-869, 1997.

[34] F. Fraternali, G. Carpentieri, A. Amendola, On the mechanical modeling of the extreme softening/stiffening response of axially loaded tensegrity prisms. *Journal of the Mechanics and Physics of Solids*, **74**, 136-157, 2015.

[35] A. Amendola, E.H. Nava, R. Goodall, I. Todd, R.E. Skelton, F. Fraternali, On the additive manufacturing, post-tensioning and testing of bi-material tensegrity structures*, Composite Structures*, **131**, 66-71, 2015.

[36] D. Ngo, F. Fraternali, C. Daraio, Highly Nonlinear Solitary Wave Propagation in Y-Shaped Granular Crystals with Variable Branch Angles. Physical Review E, **85**, 036602-1-10, 2012.

[37] R.E. Skelton, F. Fraternali, G. Carpentieri, A. Micheletti, Minimum mass design of tensegrity bridges with parametric architecture and multiscale complexity. *Mechanics Research Communications*, 58, 124-132, 2014.

[38] A. Leonard, F. Fraternali, C. Daraio, Directional wave propagation in a highly nonlinear square packing of spheres. *Experimental Mechanics*, **53**(3), 327-337, 2013.

[39] F. Fraternali, G. Carpentieri, A. Amendola, R.E. Skelton, V. F. Nesterenko, Multiscale tunability of solitary wave dynamics in tensegrity metamaterials. *Applied Physics Letters*, **105**, 201903, 2014.

[40] F. Fraternali, I. Farina, C. Polzone, E. Pagliuca, L. Feo, On the use of R-PET strips for the reinforcement of cement mortars. *Composites. Part B*, **46**, 207-210, 2013.

[41] J.R. Raney, F. Fraternali, A. Amendola, C. Daraio, Modeling and In Situ Identification of Material Parameters for Layered Structures based on Carbon Nanotube Arrays. *Composite Structures*, **93**, 3013–3018, 2011.

[42] G. Lomiento , N. Bonessio, G. Benzoni, Friction Model for Sliding Bearings under Seismic Excitation, Journal of Earthquake Engineering, **17**(8):1162-1191, 2013.

[43] M. Budek, M. J. N. Priestley, G. Benzoni, The Effect of External Confinement on Flexural Hinging in Drilled Pile Shafts, *Earthquake Spectra*, **20** (1), 1-24, 2004.

[44] Hae-Bum Yun, Sami F. Masri, Raymond W. Wolfe, Gianmario Benzoni , Data-driven methodologies for change detection in large-scale nonlinear dampers with noisy measurements, *Journal of Sound and Vibration*, **322**, Issues 1–2, 24 April 2009, Pages 336–357.

[45] D. D'Ayala, G. Benzoni, Historic and Traditional Structures during the 2010 Chile Earthquake: Observations, Codes, and Conservation Strategies. *Earthquake Spectra*, **28** (S1), S425-S451, 2012.

[46] N. Bonessio, G. Lomiento, G. Benzoni, Damage identification procedure for seismically isolated bridges, *Structural Control Health Monitoring*, **19**(5), 565–578, 2012.

[47] G. Benzoni, C. Casarotti , Effects of Vertical Load, Strain Rate and Cycling on the Response of Lead-Rubber Seismic Isolators, *Journal of Earthquake Engineering* ,**13**, 2009.

[48] A. Budek-Schmeisser, G. Benzoni, Rational seismic design of precast, prestressed concrete piles, *PCI Journal*, **53**(5), 40-53, 2008.

[49] G. Benzoni, M. J. N. Priestley, Seismic response of linked marginal wharf segments, *Journal of Earthquake Engineering* **74**, 513-539, 2003.

[50] F. Fraternali, S. Spadea, V.P. Berardi, Effects of recycled PET fibers on the mechanical properties and seawater curing of Portland cement-based concretes. *Construction and Building Materials*, **61**, 293-302, 2014.

[51] I. Farina, F. Fabbrocino, G. Carpentieri, M. Modano, A. Amendola, R. Goodall, L. Feo, F. Fraternali, *On the reinforcement of cement mortars through 3D printed polymeric and metallic fibers,* Composites Part B: Engineering, **90**, 76-85, 2016

[52] T. Blesgen, F. Fraternali, J.R. Raney, A. Amendola, C. Daraio, Continuum Limits of Bistable Spring Models of Carbon Nanotube Arrays accounting for Material Damage. *Mechanics Research Communications*, **45**, 58-63, 2012.

[53] F. Fraternali. A Mixed Lumped Stress – Displacement Approach to the Elastic Problem of Masonry Walls. Mechanics Research Communications, **38**, 176-180, 2011.

[54] F. Fraternali, M. Negri, M. Ortiz, On the Convergence of 3D Free Discontinuity Models in Variational Fracture. *International Journal of Fracture*, **166**(1-2), 3-11, 2010.

[55] F. Fraternali, S. Spadea, L. Ascione, Buckling behavior of curved composite beams with different elastic response in tension and compression. *Composite Structures*, **100**, 280-289, 2013.

[56] C. Daraio, D . Ngo, V. F. Nesterenko, F. Fraternali, Highly Nonlinear Pulse Splitting and Recombination in a Two Dimensional Granular Network. *Physical Review E*, **82**, 036603, 2010.

[57] F. Fraternali, A. Marino, T. Elsayed, A. Della Cioppa, On the structural shape optimization via variational methods and evolutionary algorithms. Mechanics of Advanced Materials and Structures, **18**, 225-243, 2011.

[58] A. Amendola, G. Benzoni, F. Fraternali, Non-linear elastic response of layered structures, alternating pentamode lattices and confinement plates. *Composite Part B, Engineering*, Online first, DOI: 10.1016/j.compositesb.2016.10.027, 2016.

[59] F. Fraternali, G. Carpentieri, R. Montuori, A. Amendola, G. Benzoni, On the use of mechanical metamaterials for innovative seismic isolation systems, COMPDYN 2015 - 5th ECCOMAS Thematic Conference on Computational Methods in Structural Dynamics and Earthquake Engineering, 349-358.

[60] A. Amendola, C.J. Smith, R. Goodall, F. Auricchio, L. Feo, G. Benzoni, F. Fraternali, Experimental response of additively manufactured metallic pentamode materials confined between stiffening plates. *Composite Structures*, **142**, 254-262, 2016.